# Local Structure and Global Patterning of Cu²⁺ Binding in Fibrillar Amyloid-β [Aβ(1-40)] Protein

**William A. Gunderson**[1], **Jessica Hernández-Guzmán**[1], **Jesse W. Karr**[2], **Li Sun**[1], **Veronika A. Szalai**[3], and **Kurt Warncke**[1],*

[1]Department of Physics, Emory University, Atlanta, GA 30322 USA

[2]Chemistry and Biochemistry Department, Siena College, Loudenville, New York, 12211 USA

[3]Center for Nanoscale Science and Technology, National Institute of Standards and Technology, Gaithersburg, MD 20899 USA.

## Abstract

The amyloid-β (Aβ) protein forms fibrils and higher-order plaque aggregates in Alzheimer's disease (AD) brain. The copper ion, $Cu^{2+}$, is found at high concentrations in plaques, but its role in AD etiology is unclear. We use high-resolution pulsed-electron paramagnetic resonance (EPR) spectroscopy to characterize the coordination structure of $Cu^{2+}$ in the fibrillar form of full-length Aβ(1-40). The results reveal a bis-*cis*-histidine (His) equatorial $Cu^{2+}$ coordination geometry, and participation of all three N-terminal His residues in $Cu^{2+}$ binding. A model is proposed, in which $Cu^{2+}$–His6/His13 and $Cu^{2+}$–His6/His14 sites alternate along the fibril axis, on opposite sides of the β-sheet fibril structure. The local intra-β-strand coordination structure is not conducive to $Cu^{2+}/Cu^{1+}$ redox-linked coordination changes, and the global arrangement of Cu sites precludes facile multi-electron and bridged-metal site reactivity. This indicates that the fibrillar form of Aβ suppresses Cu redox cycling and reactive oxygen species (ROS) production. The insulator configuration suggests application of $Cu^{2+}$-Aβ fibrils as an amyloid architecture for switchable electron charge/spin coupling and redox reactivity.

## INTRODUCTION

Alzheimer's disease (AD) is a neurodegenerative disorder of present and acute future human impact.[1] The AD brain is characterized by extracellular histopathological lesions, or plaques.[2] The primary component of the plaques is the amyloid-β (Aβ) peptide. The Aβ peptides are *n*=39-42 amino acids in length, and are denoted Aβ(1-*n*). Aβ in the plaques is predominantly in the form of amyloid fibrils, which aggregate to form higher-order structures. High-resolution solid-state nuclear magnetic resonance (SS-NMR) studies have led to molecular models for the structure of residues 9-40 of the de-metallated Aβ(1-40) fibril prepared under different conditions,[3-5] and the Aβ(1-42) fibril,[6] in which β-strand structure in central and C-terminal regions of the peptide promotes stacking of the β-turn β-fold in a parallel, in-register β-sheet arrangement. The β-sheet structure can extend along the fibril axis to micrometer lengths. The metal ion, $Cu^{2+}$, is found at high concentrations of up to 400 μM in plaques, and it is directly coordinated by the Aβ peptide.[7-10] Reactive oxygen

*Corresponding Author*: Kurt Warncke Department of Physics N201 Mathematics and Science Center 400 Dowman Drive Emory University Atlanta, Georgia 30322-2430 kwarncke@physics.emory.edu Phone: 404-727-2975 Fax: 404-727-0873.

species (ROS) generation by $Cu^{2+}$-Aβ, and ensuing oxidative damage to cellular components, has been proposed to contribute to the etiology of AD,[8,11,12] but a specific role of fibril-bound $Cu^{2+}$ (promoting or ameliorating) has remained unclear.[7,8,11,13,14] Mounting refined evidence that relatively low molecular mass oligomers are cytotoxic forms of Aβ,[6,15,16] possibly abetted by enhanced $Cu^{2+}$-promoted ROS generation,[14,17] re-invigorates the question: What is the role of fibrillar $Cu^{2+}$-Aβ in AD?

General features of $Cu^{2+}$ coordination in the soluble and fibrillar forms of Aβ(1-40) or Aβ(1-42) at pH 7.2-7.4 have been addressed by using continuous-wave EPR[18,19] and SS-NMR[10] spectroscopies. The EPR parameters, $g_\perp$, $g_\parallel$, and the copper hyperfine coupling constant, $A_\parallel$, of $Cu^{2+}$ complexed with soluble Aβ(1-16), Aβ(1-28), and monomeric Aβ(1-40) and Aβ(1-42) are the same to within experimental uncertainty.[18,19] The EPR line shape of the initially monomeric $Cu^{2+}$-Aβ(1-40) complex did not change[18] during fibrillization in the presence of $Cu^{2+}$. Transmission electron microscopy (TEM) and SS-NMR showed that the presence of $Cu^{2+}$ during Aβ(1-40) fibril formation did not influence the fibril morphology or reorganize the parallel, in-register β-sheet structure in Aβ(1-40) fibrils.[10] These results show that the $Cu^{2+}$ sites in soluble monomeric and fibrillar forms of Aβ are geometrically comparable, may involve identical or chemically-similar ligands, and that the structure of the N-terminal domain that binds $Cu^{2+}$, and the distal β-sheet-forming domains of full-length Aβ, are independent.

The detailed coordination structure of $Cu^{2+}$ in the *soluble* (non-aggregating, non-fibril forming), monomeric complexes of $Cu^{2+}$ with the truncated Aβ-peptides, Aβ(1-16)[20-25] and Aβ (1-28),[19,26] or both,[27] has been addressed by using electron spin echo envelope modulation (ESEEM) and hyperfine sublevel correlation (HYSCORE) spectroscopies, in conjunction with isotopic labeling, His-to-Ala mutations, and chemical modification. The N-terminal metal binding domain in the Aβ peptide contains three histidine (His) residues, His6, His13, and His14, all of which have been implicated in $Cu^{2+}$ coordination in soluble Aβ(1-16) and Aβ(1-28). A model of a two-component (Component Ia, Ib; Scheme 1), approximately equimolar mixture of His6/His13- and His6/His14-$Cu^{2+}$ coordination in soluble Aβ(1-16) was proposed,[22] and later revised and extended by additional spectroscopic studies.[23-25,28]

We have used high-resolution pulsed-electron paramagnetic resonance (EPR) spectroscopy to probe histidine (His) coordination of $Cu^{2+}$ (electron spin, $S$=1/2; nuclear spin, $I$=3/2) in frozen solution samples of fibrillar Aβ(1-40), to determine the local coordination structure and global patterning of $Cu^{2+}$ binding at the N-terminus of fibrillar Aβ(1-40). The results provide molecular-level insights into the chemistry and physiological impact of $Cu^{2+}$ binding by Aβ fibrils, and suggest applications of $Cu^{2+}$-Aβ(1-40) as an amyloid architecture[29] for designed, switchable electron charge/spin conduction and redox reactivity.

## MATERIALS AND METHODS

### Sample Preparation

Wild type Aβ(1–16) and Aβ(1–40) peptides were purchased from rPeptide (Athens, GA) or Bachem (King of Prussia, PA). Glycerol, sodium phosphate (NaP$_i$), sodium chloride, phosphotungstic acid (PTA), and 1,1,1,3,3,3 hexafluro-2-proponal (HFIP) were purchased from Fisher Scientific (Pittsburgh, PA). $Cu^{2+}$-Aβ samples were prepared as described previously.[18] Briefly, Aβ(1–40) peptides were monomerized with HFIP and stored at −80 °C. An aliquot of the stock solution was removed for determination of the concentration, by using a bovine serum albumin calibration curve. Fibrillar Aβ(1–40) were prepared by using 100 μM Aβ(1–40) peptide in 50 mM NaP$_i$ and 75 mM NaCl (pH 7.2), which was incubated at 37 °C for 7-14 days under quiescent conditions in the presence of equimolar $Cu^{2+}$.

Progress of fibril formation was assayed by TEM. Samples for EPR experiments were separated from the supernatant and concentrated by centrifugation of the pooled volumes in a microfuge (60 min, 16000 rcf), resuspended and washed with buffer, centrifuged a second time (30 min, 16000 rcf) and resuspended in a buffer of 50 mM $NaP_i$ and 75 mM NaCl (pH 7.2) containing 50% glycerol (v/v). Samples of the soluble Aβ(1-16) were prepared by resuspending dried peptide in buffer containing 50 mM $NaP_i$, 75 mM NaCl (pH 7.2), and 50% glycerol (v/v). An equimolar amount of $Cu^{2+}$ was added to the sample prior to freezing in liquid nitrogen.

## EPR Spectroscopy and Simulations

CW-EPR spectroscopic measurements were made by using a Bruker ELEXSYS E500 EPR spectrometer with an ER 4123SHQE X-band cavity resonator and a Bruker ER 4131VT liquid nitrogen flow temperature control system. Spectra were acquired at 120 K under non-saturating conditions.

CW-EPR simulations were performed by using the SpinCount software package (M. Hendrich, Carnegie Mellon University: www.chem.cmu.edu/groups/hendrich/facilities/index.html) by diagonalization of the following spin Hamiltonian:

$$H = \beta_e \boldsymbol{B} \cdot \boldsymbol{g} \cdot S + hS \cdot \boldsymbol{A} \cdot I \quad (1)$$

with $S = 1/2$ and $I = 3/2$ for $Cu^{2+}$. In Eq. 1, $S$ and $I$ are the electron and nuclear spin operators, $g$ and $A$ are the electron $g$ and $Cu^{2+}$ hyperfine tensors, $\beta_e$ is the Bohr magneton, $\boldsymbol{B}$ is the applied magnetic field, and $h$ is Planck's constant.

## ESEEM Spectroscopy and Simulations

ESEEM was collected at 6 K on a home-designed and constructed pulsed EPR spectrometer using the three-pulse (π/2-$\tau$-π/2-$T$-π/2-$\tau$-echo) microwave pulse sequence.[30] ESEEM waveforms were cosine Fourier transformed to generate ESEEM frequency spectra. Data processing and analysis was performed by using codes written in Matlab (Mathworks, Natick, MA). All spectra were recorded under the same conditions, with $B_0$ = 303.0 mT and $\tau$ = 310 ns. The $\tau$ value of 310 ns was chosen to suppress the undesired modulation from $^1$H shf coupling, and to enhance the contribution of the $^{14}$N $\Delta m_I = \pm 2$ ($2\nu_{dq}$) combination modulation.

Numerical simulations of the ESEEM were performed by using the OPTESIM software package.[31] The spin Hamiltonian for the $Cu^{2+}$–$^{14}$N interaction is:

$$H = -g_n \beta_n \boldsymbol{B} \cdot I + hS \cdot \boldsymbol{A} \cdot I + I' \cdot \boldsymbol{Q} \cdot I' \quad (2)$$

where $A$ is the shf coupling tensor, $Q$ is the nqi tensor, $g_n$ is the nuclear $g$ factor, $\beta_n$ is the nuclear magneton, $\boldsymbol{B}$ is the applied magnetic field, and $h$ is Planck's constant. The traceless tensor $Q$ is related to the nuclear quadrupole coupling constant, $e^2qQ/h$, and the electric field gradient asymmetry parameter, $\eta$, as follows:

$$Q_{zz} = \frac{e^2qQ}{2I(2I-1)h} \quad (3)$$

$$\eta = \frac{Q_{xx} - Q_{yy}}{Q_{zz}} \quad (4)$$

where $e$ is the elementary charge, $q$ is the electric field gradient, and $Q$ is the nuclear quadrupole moment. The relative orientation of the PAS of the nqi and shf tensors is defined by the Euler angles $[\alpha_Q, \beta_Q, \gamma_Q]$. For systems with >1 coupled $^{14}$N nucleus, the orientation of the shf tensors is defined by the Euler angles, $[\alpha_A, \beta_A, \gamma_A]$. Hybrid optimization in the simulations was performed by sequential application of genetic and Nelder-Mead simplex algorithms.[31]

## RESULTS AND DISCUSSION

## EPR spectroscopy of natural isotopic abundance fibrillar $Cu^{2+}$-Aβ(1-40) and soluble $Cu^{2+}$-Aβ(1-16)

Continuous-wave (CW)-EPR spectra of the soluble $Cu^{2+}$-Aβ(1-16) and fibrillar $Cu^{2+}$-Aβ(1-40) complexes are shown in Figure 1. The EPR spectra of the two complexes are closely similar, as quantified by the EPR simulations (Figure 1, A and B; dashed lines), and simulation parameters, which are presented in Table 1. The single set of $g_\perp$, $g_\parallel$ and $A_\perp$, $A_\parallel$ values required in the simulations are the same for the Aβ(1-16) and Aβ(1-40) complexes, to within one standard deviation. The $g_\parallel$ and $A_\parallel$ parameters in Table 1 are typical of a tetragonal, type-2 $Cu^{2+}$ center.[32] A three-nitrogen/one-oxygen (3N1O) equatorial coordination of $Cu^{2+}$ is suggested by the Peisach-Blumberg correlation of $g_\parallel$ and $A_\parallel$.[33]

The EPR simulation parameters ($g_\parallel$=2.272, $g_\perp$=2.056, $A_\parallel$=527 MHz) reported here for the fibrillar $Cu^{2+}$-Aβ(1-40) complex are comparable with values reported previously for $Cu^{2+}$ in soluble Aβ(1-40) ($g_\parallel$=2.268, $g_\perp$=2.061, $A_\parallel$=534 MHz)[18] and in fibrillar Aβ(1-40/42) ($g_\parallel$=2.268, $g_\perp$=2.061, $A_\parallel$=534 MHz).[18,19] These parameters are also comparable to those for Component I of $Cu^{2+}$-Aβ(1-16). Our results, in agreement with the previous EPR studies,[18,19] thus indicate that the $Cu^{2+}$ site in fibrillar Aβ(1-40) has a comparable geometry and set of equatorial ligand atoms, as for Component I in $Cu^{2+}$-Aβ(1-16).

The CW-EPR spectra of the fibrillar $^{13}C,^{15}$N-His13-$Cu^{2+}$-Aβ(1-40) and $^{13}C,^{15}$N-His14-$Cu^{2+}$-Aβ(1-40) complexes are shown in Figure 1, C and D. The EPR line shapes of the isotope-labeled complexes are comparable to the line shapes for the natural isotopic abundance spectra. Although hyperfine coupling with the $I$=3/2 copper nucleus is displayed at $g_\parallel$, an influence of the change from $^{12}$C ($I$=0) to $^{13}$C ($I$=1/2), and from $^{14}$N ($I$=1) to $^{15}$N ($I$=1/2), on the EPR line shape is not apparent, owing to inhomogeneous broadening. High resolution techniques of EPR spectroscopy, such as ESEEM, are necessary to resolve the ligand superhyperfine coupling.

## $^{14}$N ESEEM spectroscopy of natural isotopic abundance fibrillar $Cu^{2+}$-Aβ(1-40) and soluble $Cu^{2+}$-Aβ(1-16)

Three-pulse ESEEM waveforms and corresponding cosine Fourier transform (FT) spectra of four $Cu^{2+}$-Aβ complexes, are shown in Figures 2 and 3, respectively. The spectral features are from the "remote," non-coordinated $^{14}$N of His imidazole, and are characteristic of the "exact cancellation" condition[34] for coupling of the unpaired electron spin from $Cu^{2+}$ with $^{14}$N. The $\nu_0$, $\nu_-$ and $\nu_+$ "pure" nuclear quadrupole interaction (nqi) frequencies, and the frequencies of the $\Delta m_I = \pm 1$, and $\Delta m_I = \pm 2$ (double quantum, $\nu_{dq}$) transitions, that originate from the non-cancellation electron spin manifold, and that include both nqi and superhyperfine (shf) contributions, are identified in Figure 3. Multiple $^{14}$N couplings result in the presence of weak modulation at sums of the fundamental modulation periods.[34,35] The "combination lines" are denoted in the FT spectra in Figure 3. In addition to the combination lines at the nuclear quadrupole frequencies, a broad feature centered at 7.8 MHz is observed, that corresponds to the $2\nu_{dq}$, double quantum combination line.[31] Combination features of

order >2 are not observed. The spectra in Figure 3 thus indicate that two histidines coordinate $Cu^{2+}$ in fibrillar Aβ(1-40).

[14]N ESEEM simulations for the fibrillar $Cu^{2+}$-Aβ(1-40) and soluble $Cu^{2+}$-Aβ(1-16) complexes are shown as dashed lines in Figure 3. Simulations were obtained by using the hybrid optimization protocol in the OPTESIM software.[31] Simulation parameters are presented in Table 2. Simulation of the ESEEM was optimized by using a minimal set of two coupled [14]N. The simulation parameters for the fibrillar $Cu^{2+}$-Aβ(1-40) and soluble $Cu^{2+}$-Aβ(1-16) complexes are the same, to within the 99% confidence interval, with the exception of the $A_{xx}$, parameter, which deviates from overlap of the confidence regions by 0.015 MHz, or 1.3%. The simulations indicate that interactions of the coordinating bis-His-imidazole side chains with $Cu^{2+}$ in the fibrillar Aβ(1-40) and soluble Aβ(1-16) complexes are comparable, and suggest that the physical-chemical properties of the other ligands involved in $Cu^{2+}$ coordination are also comparable.

The line shape of the $2\nu_{dq}$ feature depends sensitively on the coordination geometry and relative orientation of the His imidazole rings.[31] The Euler angles, $[\alpha_A \beta_A \gamma_A]$, for the relative orientation of the two ^{14}N shf principal axis systems (PAS), specify *cis*-coordination of $Cu^{2+}$ by the two His imidazole in fibrillar $Cu^{2+}$-Aβ(1-40), and also directly confirm the bis-*cis*-His coordination proposed for soluble $Cu^{2+}$-Aβ(1-16) Component I.[21,22,24] This is illustrated in Figure 4 by the approximately orthogonal *x*-axes. The *x*-axis of the dipolar shf PAS lies in the imidazole ring plane, and is directed at an angle of 13°, relative to the imidazole N-N axis.[36] The *x*-axis thus points roughly toward the coordinated $Cu^{2+}$. The *z*-axis is directed approximately perpendicular to the imidazole ring plane, at an angle of 4° with respect to the ring plane normal.[36] Thus, Figure 4 also indicates that the imidazole rings are tilted by about 90°, with respect to each other. The robustness of the bis-*cis*-His assignment is shown by the dramatically different waveforms and line shapes of the $2\nu_{dq}$ feature in different geometries (Supporting Information, Figures S1 and S2).

## Influence of Selective ^{15}N-Substitution of Histidine Residues on ^{14}N ESEEM from $Cu^{2+}$ Bound to Fibrillar Aβ(1-40)

Figures 2 and 3 show the ESEEM waveforms and cosine FT spectra for the $Cu^{2+}$-Aβ(1-40) complexes with ^{15}N-imidazole ring-labeled His13 and His14. Under the exact cancellation condition [$\nu_N = A/2$, where $\nu_N$ is the nuclear Larmor frequency and $A$ is the shf coupling constant], substitution of [14]N ($I=1$; nqi present) with [15]N ($I=1/2$; no nqi) results in a dramatic change in the ESEEM from the coupled nitrogen.[34] The dominant isotropic contribution to the shf coupling of the remote imidazole nitrogen is expected to lead to a doublet line shape in the FT spectrum upon ^{15}N-substitution, with dipolar shf-broadened features near $\nu_N - A/2 \approx 0$ and $\nu_N + A/2 \approx 2\nu_N$, that replace the narrow, large-amplitude $\nu_0$, $\nu_-$ and $\nu_+$ nqi lines, and distinctive $\nu_{dq}$ line, that are characteristic of the ^{14}N shf coupling. In addition, ESEEM amplitudes are dependent on the degree of nuclear state mixing,[37] which is strong for ^{14}N coupling, because of the combined nuclear quadrupole and shf interactions, with generally non-coincident PAS.[34] In contrast, mixing is relatively weaker for ^{15}N coupling. Thus, the ^{15}N ESEEM may not be resolved at modest signal-to-noise ratios, in the presence of exact cancellation ESEEM from other coupled, ^{14}N-nitrogen nuclei.[38] This is the case in Figures 2 and 3. The predominant effect of ^{15}N-substitution is, therefore, to eliminate the strong exact cancellation ESEEM from the ^{14}N that is replaced.[38] Thus, the qualitatively comparable ESEEM for the ^{15}N-imidazole-labeled and natural abundance fibrillar $Cu^{2+}$-Aβ(1-40) complexes eliminates a single equatorial bis-His coordination mode for $Cu^{2+}$, because all ^{14}N combination features would be lost upon ^{15}N-substitution on His13 or His14. This is exemplified by simulations of single- and bis-*cis*- imidazole coordinated ^{14}N in Supporting Information, Figures S3 and S4. Therefore, a single bis-His

coordination mode by the following combinations is ruled out: His6/His13, His6/His14, or His13/His14.

The effects of $^{15}$N-substitution are revealed by division of the waveform from the $^{15}$N-labeled samples by the all-$^{14}$N-His waveform. As shown in Figure 5, weak modulation in the quotient waveform is present, with peaks and troughs at positions that correspond to the features in the individual ESEEM waveforms, but with opposite phase. This quotient waveform is consistent with the $^{15}$N-substitution, because the waveform in the numerator of the envelope division includes reduced contributions from coupled $^{14}$N, relative to the waveform in the denominator. The shf and nqi simulation parameters, obtained for the natural abundance $Cu^{2+}$-Aβ(1-40) complex in Table 2, were used to perform an ESEEM simulation analysis of the effect of $^{15}$N-substitution on a minimal model of two equimolar pairs of bis-*cis*-His-$Cu^{2+}$ sites. The simulated quotient waveform in Supporting Information, Figure S5, which is obtained from the division of a 1:1 mixture of [$^{15}$N, $^{14}$N] and [$^{14}$N, $^{14}$N] sites by the all-$^{14}$N model, shows weak, negative-phase modulation, with opposite-phase peaks and troughs at positions that correspond to features in the individual simulated ESEEM waveforms. The quotient simulation thus agrees with the experimental quotient ESEEM in Figure 5.

The results and quotient ESEEM analysis are consistent with the approximately equimolar mixture of $Cu^{2+}$-coordinating bis-His pairs, [His6/His13, His6/His14], in the fibril. This is consistent with the approximately equimolar His6/His13 and His6/H14 contributions in the Component Ia, Ib model proposed for soluble $Cu^{2+}$-Aβ(1-16),[22] and other soluble $Cu^{2+}$-Aβ complexes.[24,26]

## Model for $Cu^{2+}$ coordination in fibrillar Aβ(1-40)

We propose a [His6/His13, His6/His14] model for His coordination of $Cu^{2+}$ in fibrillar Aβ(1-40), as illustrated in Figure 6. The structure of residues 9-40 in the model is based on the Aβ(1-40) fibril structure determined by SS-NMR (Protein Data Bank ID: 2LMN).[3] All atoms of residues 15-40 and backbone atoms of residues 9-14 were fixed in the model. Residues 1-8 are disordered (absent) in the 2LMN structure.[3] Therefore, the dihedral angles of residues 1-8, and side chain dihedral angles of residues 1-14, were adjusted at the N-termini of the β-strands of 2LMN, according to the following considerations: (1) equatorial coordination by bis-*cis*-histidine, terminal-amine, and Ala2 carbonyl (as in Scheme 1), and (2) adherence to local steric constraints. The molecular visualization program, PyMOL (www.pymol.org), was used in model building. At the local level of the $Cu^{2+}$ sites, the model is consistent with the paramagnetic quenching of the imidazole ring $^{13}$Cε and $^{13}$Cδ features in the CPMAS SS-NMR studies of either $^{13}$C-labeled- His13 or His14, which was reported as 30-60% (corresponding to 40-70% of narrow-line amplitude maintained).[10] In addition, the model incorporates the symmetry of the imidazole ring $^{13}$C quenching determined by SS-NMR, which was Cε=Cδ>Cγ, and which indicated that His13 and His14 coordinate $Cu^{2+}$ through the imidazole ring Nε.[10] Although we cannot rigorously rule out $Cu^{2+}$ coordination by a His13/His14 sub-population, as proposed for soluble Aβ(1-16),[21] a His13–$Cu^{2+}$–His14 complex would severely distort the β-strand structure of the liganding peptide around residues 13 and 14. This is because His13 and His14 are part of the β-strand region in the fibrils, and therefore, the imidazole rings extend from opposite sides of the β-sheet[3]. This is supported by the conclusions of the SS-NMR study,[10] and TEM and CW-EPR studies,[18] that $Cu^{2+}$ binding in fibrils does not alter the parallel, in-register β-sheet structure.

The model in Figure 6 is consistent with previous studies,[18,19] which concluded that the $Cu^{2+}$-binding, N-terminal domain of Aβ was structurally independent from the β-sheet-forming central and C-terminal regions. Thus, the coordination geometry and atom-types of

the non-His equatorial ligands of the $Cu^{2+}$ site in the soluble complexes with Aβ(1-16) and Aβ(1-28), appear to be maintained in fibrils. We again note that the His13 and His14 side chains are constrained by the β-strand structure of the fibrils to protrude from opposite sides of the β-sheet.[3-5] Therefore, the bis-*cis*-His6/His13-$Cu^{2+}$ and bis-*cis*-His6/His14-$Cu^{2+}$ sites are positioned on different β-sheet faces, and this pattern alternates along the fibril axis, as shown in Figure 6. The proposed alternating arrangement of sites separates $Cu^{2+}$ beyond the ~7 Å limit of detectable dipolar broadening of the EPR spectrum.[19] There is no evidence in the CW-EPR spectra for electron spin exchange-induced broadening. The shortest $Cu^{2+}$–$Cu^{2+}$ separation distance in the model is 11 Å, along the direction of the fibril axis. As depicted in Figure 6, this arrangement also suppresses the inter-β-strand coordination of $Cu^{2+}$, which is consistent with earlier evidence against this binding mode,[19] and with the general absence of $Cu^{2+}$ binding effects on the structure of the demetallated fibril,[18] Thus, in our view, the approximately isoenergetic Component Ia and Ib $Cu^{2+}$ binding modes, that are identified in the soluble Aβ(1-16) peptide fragment,[22,23] are a manifestation of the alternating site structure of $Cu^{2+}$ binding in fibrillar full-length Aβ. Owing to the parallel, in-register stacking of the β-turn-β fold of Aβ(1-40) peptides in all reported high resolution fibril structures,[3-5] the alternating pattern of N-terminal $Cu^{2+}$ sites displayed in Figure 6 is expected to be a characteristic feature of $Cu^{2+}$–Aβ(1-40) fibril polymorphs.

## Implications of $Cu^{2+}$-His coordination geometry and the patterning of Cu sites in fibrillar Aβ for dioxygen reactivity and ROS generation

Reported pro- and anti-oxidant properties of Aβ are dependent upon the specific measurement conditions and the peptide concentration.[12,14] Any cytotoxicity of the Cu-Aβ complex, relative to the demetallated peptide, is thought to be caused by $Cu^{1+}$-mediated reduction of dioxygen ($O_2$), to produce hydrogen peroxide ($H_2O_2$) and other ROS, which is accompanied by $Cu^{2+}/Cu^{1+}$ redox cycling.[8,12,14,39] The coordination geometry of $Cu^{1+}$ is bis-*trans*-His in the soluble monomeric Aβ(1-16) and Aβ(1-40) complexes[40] and in smaller soluble Aβ peptides.[41] A His13–$Cu^{1+}$–His14 dyad was assigned.[40,41] The linear coordination mode is consistent with the preference for $Cu^{1+}$ bis-*trans*-His geometry in the histidyl-histidine dipeptide[42] and model imidazole complexes.[43-45] The bis-*cis*-His Cu coordination by sequence-distant His pairs, in the model in Figure 6, precludes facile $Cu^{1+}$ coordination by the sequence-adjacent His13-His14 dyad. Thus, $Cu^{2+}$ reduction to linear $Cu^{1+}$ can be achieved only at large inner sphere[40,46] and outer sphere reorganization energies, which would substantially decrease the rate of reduction. The model in Figure 6 also spatially segregates the His imidazole side chains in each peptide into either [His6/His13, His14] or [His6/His14, His13]. This prevents facile achievement of the distorted-trigonal (or "pseudo-T-shaped") interaction of a third imidazole ligand with the dyad.[42,43] The distorted-trigonal interaction enhances the sluggish $O_2$ reactivity of linear His-$Cu^{1+}$-His in models[45] and in monomeric Aβ.[17] Thus, factors that would promote reoxidation of a linear His-$Cu^{1+}$-His, if formed at equilibrium in fibrillar Aβ(1-40),[47] are absent. As shown in Figure 6, the alternating pattern of Cu sites in fibrillar Aβ(1-40) also constrains formation of inter-peptide ligation of Cu, and maintains a minimum Cu-Cu distance of approximately 11 Å. This eliminates multi-electron redox reactivity and bridged-metal site chemistry.[41] For example, a two-electron, two-proton process is proposed for ROS generation by Cu in soluble Aβ(1-16),[14] and Cu-Cu distances in oxygen-activating enzymes are typically approximately 4.0-4.5 Å.[48] Thus, in addition to the local Cu site constraints, the global arrangement of Cu sites also acts to suppress $Cu^{2+}/Cu^{1+}$ redox cycling and ROS production. In general, reactivity of the soluble monomer, or non-fibrillar oligomers, of Aβ appears to depend on the prevalent dynamics in these forms.[39,49] Extensive configurational sampling[39,50] will be suppressed in fibrillar forms of full-length Aβ. Based on the model in Figure 5, and the body of results considered above, we propose that the general physiological impact of fibrillar Aβ, at the levels of both the local Cu site coordination

structure,[17,40] and global Cu site arrangement, is suppression of Cu redox cycling and ROS production.

The amyloid protein structure provides a robust nanomaterial scaffold for templating ordered arrays of molecules to produce collective functions, including energy and charge transfer.[29,51] Metal deposition on engineered amyloid frameworks has created nanowires with relatively high conductivity.[52,53] The native $Cu^{2+}$-A$\beta$(1-40) fibril accommodates site-specific, high-density metal ion loading, restricts electronic coupling between metal sites. Mutational and chemical modifications in residues 1-8 could be used to promote metal-metal interations, by introducing accessible alternative conformations, or to integrate additional metal ion binding sites. This suggests applications of $Cu^{2+}$-A$\beta$ fibrils as tunable, and potentially switchable (enabled, for example, by metal ion concentration or pH changes), electron charge/spin conductivity and redox reactivity architectures.

## CONCLUSION

We have used $^{14}N$ ESEEM spectroscopy to address His coordination of $Cu^{2+}$ in frozen solution samples of fibrillar A$\beta$(1-40), by measuring the superhyperfine interaction of the unpaired electron spin with the remote imidazole nitrogen nucleus. Simulation analysis of the ligand geometry-dependent $2\nu_{dq}$ combination line shape reveals a bis-*cis*-His coordination of $Cu^{2+}$. The $^{14}N$ ESEEM from native and selectively $^{15}N$-His-labeled A$\beta$(1-40) indicates an approximately equimolar mixture of $Cu^{2+}$-coordinating bis-His pairs, [His6/His13, His6/His14], in the fibril. This is consistent with the approximately equimolar His6/His13 and His6/H14 contributions in the Component Ia, Ib model proposed for soluble $Cu^{2+}$-A$\beta$(1-16),[22] and other soluble $Cu^{2+}$-A$\beta$ complexes.[24,26] The ESEEM results for fibrillar $Cu^{2+}$-A$\beta$(1-40), and control $Cu^{2+}$-A$\beta$(1-16), in agreement with the previous EPR studies,[18,19] thus indicate that the $Cu^{2+}$ site in fibrillar A$\beta$(1-40) has a comparable geometry and set of equatorial ligand atoms, as for Component I in $Cu^{2+}$-A$\beta$(1-16). We propose a [His6/His13, His6/His14] model for His coordination of $Cu^{2+}$ in fibrillar A$\beta$(1-40), in which residues 1-8 are configured in accord with the EPR and ESEEM-derived constraints, and residues 9-40 assume the $\beta$-sheet structure determined by SS-NMR.[3] The fibril context dictates that the $Cu^{2+}$-bis-*cis*-His6/His13 and $Cu^{2+}$-bis-*cis*-His6/His14 sites are positioned on different $\beta$-sheet faces, and that this pattern alternates along the fibril axis. The alternating arrangement of sites separates $Cu^{2+}$ beyond the ~7 Å limit of detectable dipolar broadening of the EPR spectrum.[19] The local intra-$\beta$-strand coordination structure is not conducive to $Cu^{2+}/Cu^{1+}$ redox-linked coordination changes, and the global arrangement of Cu sites precludes facile multi-electron and bridged-metal site reactivity. It is therefore concluded that the fibrillar form of A$\beta$ suppresses Cu redox cycling and reactive oxygen species (ROS) production.

## Supplementary Material

Refer to Web version on PubMed Central for supplementary material.

## Acknowledgments

## Abbreviations

**A$\beta$**    amyloid-$\beta$ protein

| | |
|---|---|
| **AD** | Alzheimer's disease |
| **CPMAS** | Carr-Purcell magic angle spinning |
| **CW** | continuous-wave |
| **EPR** | electron paramagnetic resonance |
| **ESEEM** | electron spin echo envelope modulation |
| **EXAFS** | Extended X-ray absorption fine structure |
| **FT** | Fourier transform |
| **HYSCORE** | hyperfine sublevel correlation |
| **nqi** | nuclear quadrupole interaction |
| **OPTESIM** | optimization of ESEEM simulation |
| **PAS** | principal axis system |
| **shf** | superhyperfine |
| **ROS** | reactive oxygen species |
| **SS-NMR** | solid-state nuclear magnetic resonance |
| **TEM** | transmission electron microscopy |

## REFERENCES

1. Selkoe DJ. Nature Med. 2011; 17:1060. [PubMed: 21900936]

2. Selkoe DJ. Ann. Intern. Med. 2004; 140:627. [PubMed: 15096334]

3. Petkova AT, Yau W-M, Tycko R. Biochemistry. 2006; 45:498. [PubMed: 16401079]

4. Paravastu AK, Leapman RD, Yau W-M, Tycko R. Proc. Natl. Acad. Sci. U. S. A. 2008; 105:18349. [PubMed: 19015532]

5. Bertini I, Gonnelli L, Luchinat C, Mao J, Nesi AJ. Am. Chem. Soc. 2011; 133:16013.

6. Ahmed M, Davis J, Aucoin D, Sato T, Ahuja S, Aimoto S, Elliott JI, Van Nostrand WE, Smith SO. Nature Struct. Mol. Biol. 2010; 17:561. [PubMed: 20383142]

7. Lovell MA, Robertson JD, Teesdale WJ, Campbell JL, Markesbery WR. J. Neurol. Sci. 1998; 158:47. [PubMed: 9667777]

8. Bush AI. Trends Neurosci. 2003; 26:207. [PubMed: 12689772]

9. Miller LM, Wang Q, Telivala TP, Smith RJ, Lanzirotti A, Miklossy JJ. Struct. Biol. 2006; 155:30.

10. Parthasarathy S, Long F, Miller Y, Xiao Y, McElheny D, Thurber K, Ma B, Nussinov R, Ishii YJ. Am. Chem. Soc. 2011; 133:3390.

11. Hung YH, Bush AI, Cherny RA. J. Biol. Inorg. Chem. 2010; 15:61. [PubMed: 19862561]

12. Smith DG, Cappai R, Barnham KJ. Biochim. Biophys. Acta. 2007; 1768:1976. [PubMed: 17433250]

13. Barnham KJ, Bush AI. Curr. Op. Chem. Biol. 2008; 12:222.

14. Hureau C, Faller P. Biochimie. 2009; 91:1212. [PubMed: 19332103]

15. Ono K, Condron MM, Teplow DB. Proc. Natl. Acad. Sci. U. S. A. 2009; 106:14745. [PubMed: 19706468]

16. Walsh DM, Selkoe DJ. J. Neurochem. 2007; 101:1172. [PubMed: 17286590]

17. Shearer J, Callan PE, Tran T, Szalai VA. Chem. Commun. 2010; 46:9137.

18. Karr JW, Szalai VA. Biochemistry. 2008; 47:5006. [PubMed: 18393444]

19. Sarell CJ, Syme CD, Rigby SEJ, Viles JH. Biochemistry. 2009; 48:4388. [PubMed: 19338344]

20. Shin, B.-k.; Saxena, S. Biochemistry. 2008; 47:9117. [PubMed: 18690709]

21. Shin, B.-k.; Saxena, S. J. Phys. Chem. A. 2011; 115:9590. [PubMed: 21491887]

22. Drew SC, Noble CJ, Masters CL, Hanson GR, Barnham KJ. J. Am. Chem. Soc. 2009; 131:1195. [PubMed: 19119811]

23. Drew SC, Barnham KJ. Acc. Chem. Res. 2011; 44:1146. [PubMed: 21714485]

24. Dorlet P, Gambarelli S, Faller P, Hureau C. Angew. Chem., Int. Ed. 2009; 48:9273.

25. Alies B, Eury H, Bijani C, Rechignat L, Faller P, Hureau C. Inorg. Chem. 2011; 50:11192. [PubMed: 21980910]

26. Syme CD, Nadal RC, Rigby SEJ, Viles JH. J. Biol. Chem. 2004; 279:18169. [PubMed: 14978032]

27. Karr JW, Akintoye H, Kaupp LJ, Szalai VA. Biochemistry. 2005; 44:5478. [PubMed: 15807541]

28. El Khoury Y, Dorlet P, Faller P, Hellwig P. J. Chem. Phys. B. 2011; 115:14812.

29. Knowles TPJ, Buehler MJ. Nature Nanotech. 2011; 6:469.

30. Schweiger, A.; Jeschke, G. Principles of pulse electron paramagnetic resonance. Oxford University Press; Oxford, UK: 2001.

31. Sun L, Hernandez-Guzman J, Warncke K. J Magn Reson. 2009; 200:21. [PubMed: 19553148]

32. Wertz, JE.; Bolton, JR. Electron Spin Resonance. Chapman and Hall; New York: 1986.

33. Peisach J, Blumberg WE. Arch. Biochem. Biophys. 1974; 165:691. [PubMed: 4374138]

34. Mims WB, Peisach J. J Chem Phys. 1978; 69:4921.

35. McCracken J, Pember S, Benkovic SJ, Villafranca JJ, Miller RJ, Peisach J. J Am Chem Soc. 1988; 110:1069.

36. Colaneri MJ, Peisach JJ. Am. Chem. Soc. 1995; 117:6308.

37. Mims WB. Physical Review B. 1972; 5:2409.

38. Warncke K, Brooks HB, Babcock GT, Davidson VL, Mccracken JJ. Am. Chem. Soc. 1993; 115:6464.

39. Hureau C, Balland V, Coppel Y, Solari PL, Fonda E, Faller PJ. Biol. Inorg. Chem. 2009; 14:995.

40. Shearer J, Szalai VA. J. Am. Chem. Soc. 2008; 130:17826. [PubMed: 19035781]

41. Himes RA, Park GY, Siluvai GS, Blackburn NJ, Karlin KD. Angew. Chem., Int. Ed. 2008; 120:9224.

42. Himes RA, Park GY, Barry AN, Blackburn NJ, Karlin KD. J. Am. Chem. Soc. 2007; 129:5352. [PubMed: 17411054]

43. Sanyal I, Karlin KD, Strange JR, Blackburn NJ. J. Am. Chem. Soc. 1993; 115:11259.

44. Sorrel TN, Jameson DL. J. Am. Chem. Soc. 1983; 105:6013.

45. Le Clainche L, Giorgi M, Reinaud O. Eur. J. Inorg. Chem. 2000:1931.

46. Xie B, Elder T, Wilson LJ, Stanbury DM. Inorg. Chem. 1999; 38:12.

47. Feaga HA, Maduka RC, Foster MN, Szalai VA. Inorg. Chem. 2011; 50:1614. [PubMed: 21280585]

48. Mirica LM, Ottenwaelder X, Stack TD. Chem. Rev. 2004; 104:1013. [PubMed: 14871148]

49. Hureau C, Coppel Y, Dorlet P, Solari PL, Sayen S, Guillon E, Sabater L, Faller P. Angew. Chem., Int. Ed. 2009; 121:9686.

50. Balland V, Hureau C, Saveant J-M. Proc. Natl. Acad. Sci. U. S. A. 2010; 107:17113. [PubMed: 20858730]

51. Liang Y, Guo P, Pingali SV, Pabit S, Thiyagarajan P, Berland KM, Lynn DG. Chem. Commun. 2008:6522.

52. Scheibel T, Parthasarathy R, Sawicki G, Lin X-M, Jaeger H, Lindquist SL. Proc. Natl. Acad. Sci. U. S. A. 2003; 100:4527. [PubMed: 12672964]

53. Carny O, Shalev DE, Gazit E. Nano Lett. 2006; 6:1594. [PubMed: 16895341]
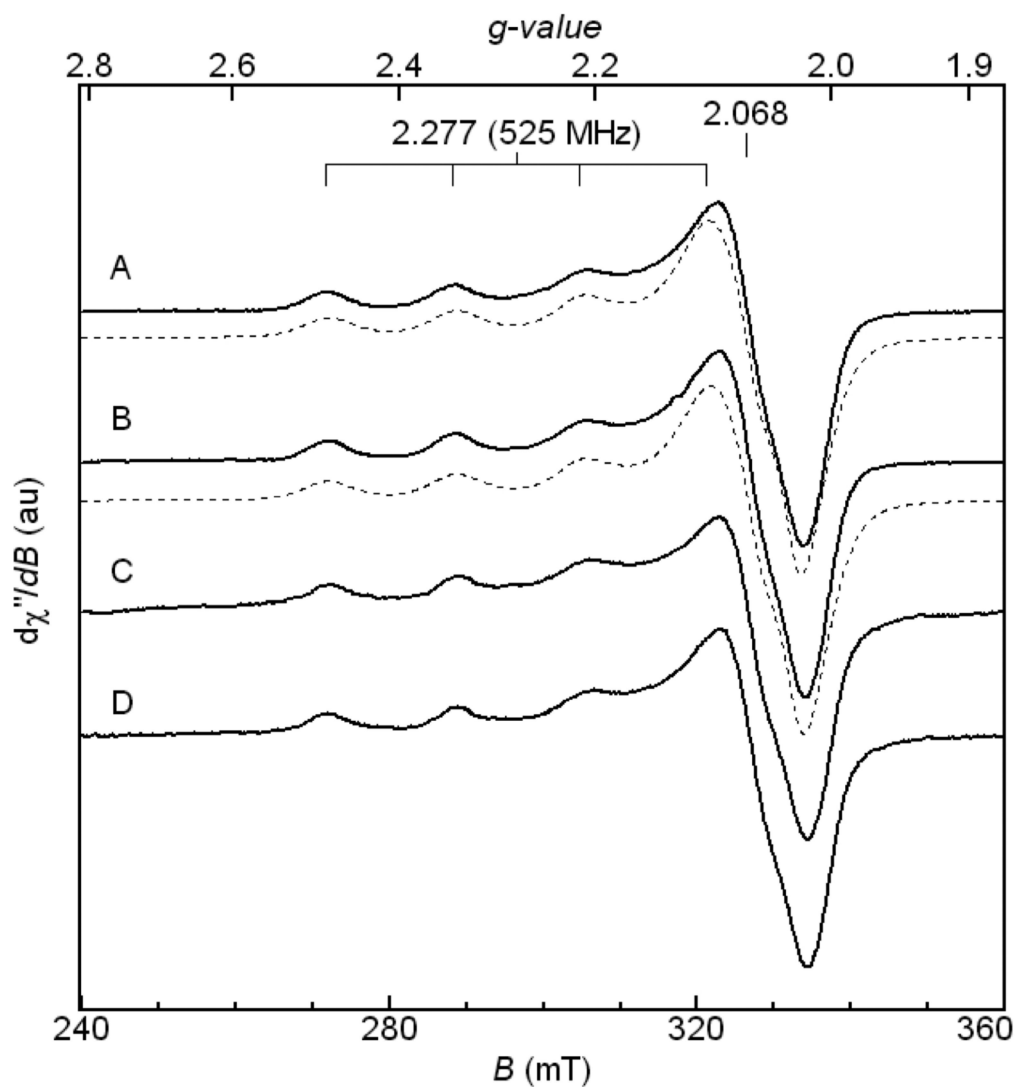
**Figure 1.**
CW-EPR spectra of $Cu^{2+}$-Aβ complexes. (A) Soluble $Cu^{2+}$-Aβ(1-16), experiment and simulation (dashed line), (B) Fibrillar $Cu^{2+}$-Aβ(1-40), experiment and simulation (dashed line), (C) $^{13}C$,$^{15}N$-His13-$Cu^{2+}$-Aβ(1-40), (D) $^{13}C$,$^{15}N$-His14-$Cu^{2+}$-Aβ(1-40). *Acquisition parameters*: microwave frequency = 9.45 GHz; microwave power = 2 mW; modulation amplitude = 1 mT; modulation frequency = 100 kHz; time constant = 10.24 ms; conversion time = 81.92 ms; $T$ = 120 K. Spectra A and B are an average of 10 scans, and spectra C and D are an average of 25 scans. Simulation parameters for spectra A and B are presented in Table 1.
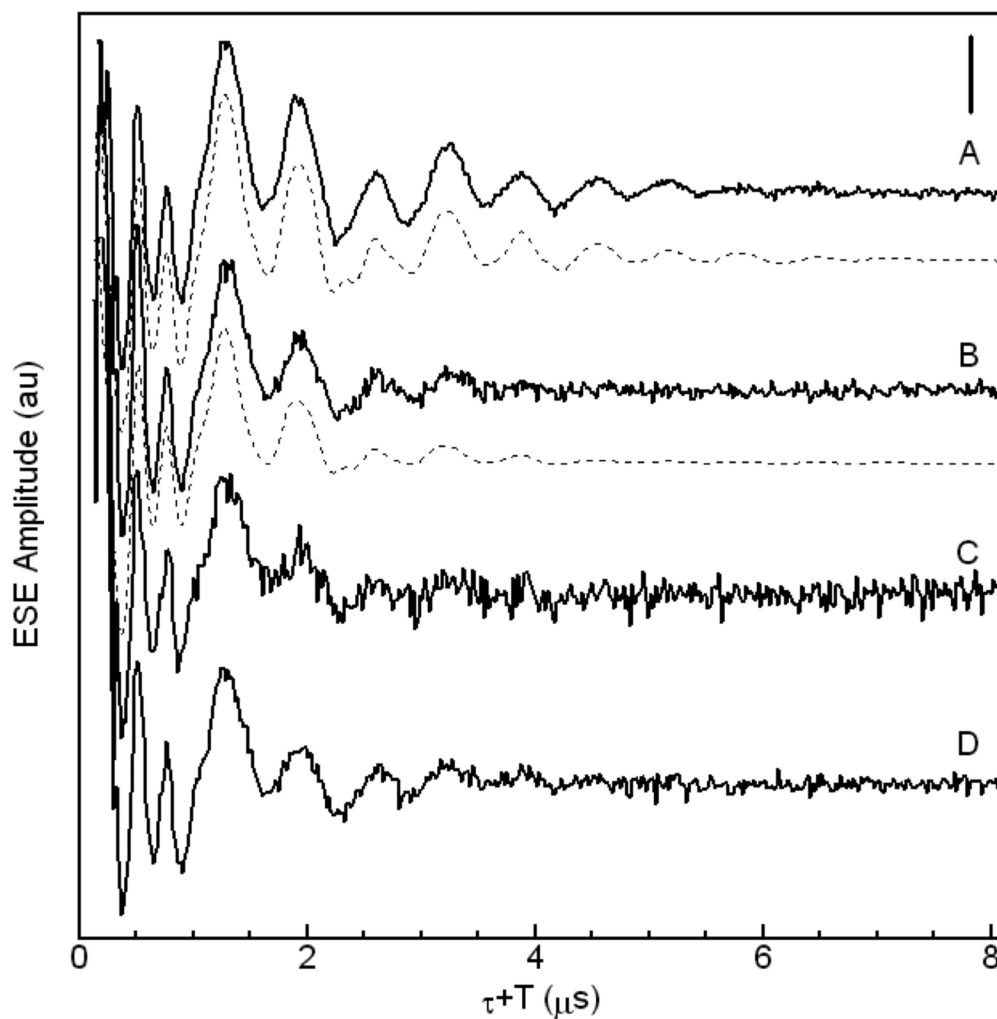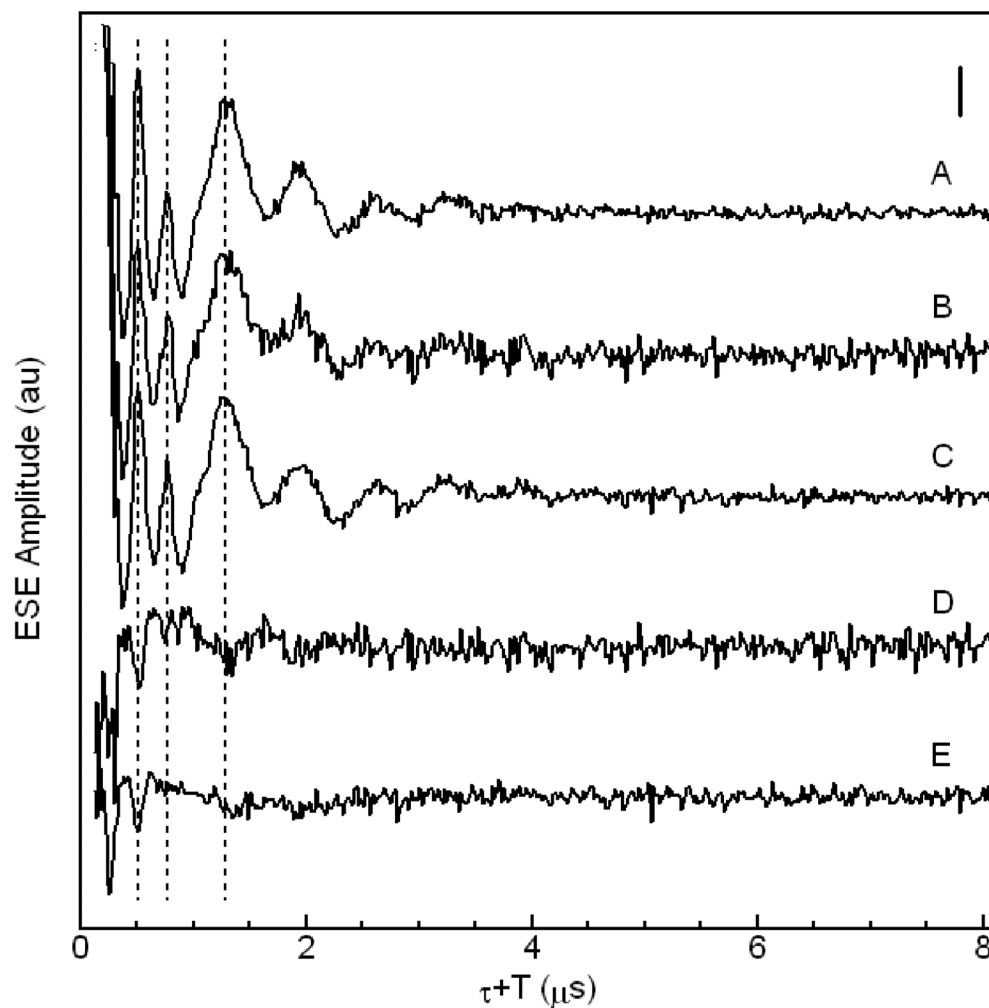
**Figure 2.**
Three-pulse ESEEM waveforms of $Cu^{2+}$-Aβ complexes. (A) Soluble $Cu^{2+}$-Aβ(1-16), experiment and simulation (dashed line), (B) Fibrillar $Cu^{2+}$-Aβ(1-40), experiment and simulation (dashed line), (C) $^{13}C,^{15}N$-His13-$Cu^{2+}$-Aβ(1-40), (D) $^{13}C,^{15}N$-His14-$Cu^{2+}$-Aβ(1-40). The vertical scale bar corresponds to 25% of the echo amplitude at $\tau + T = 8$ μs. *Acquisition Parameters*: microwave frequency, 8.750 GHz, $B_0 = 303.0$ mT, $T = 6$ K, $\tau = 310$ ns. Spectrum A is an average of 10 scans, spectrum B is an average of 16 scans, and spectra C and D are an average of 25 scans. Simulation parameters for waveforms A and B are presented in Table 2.
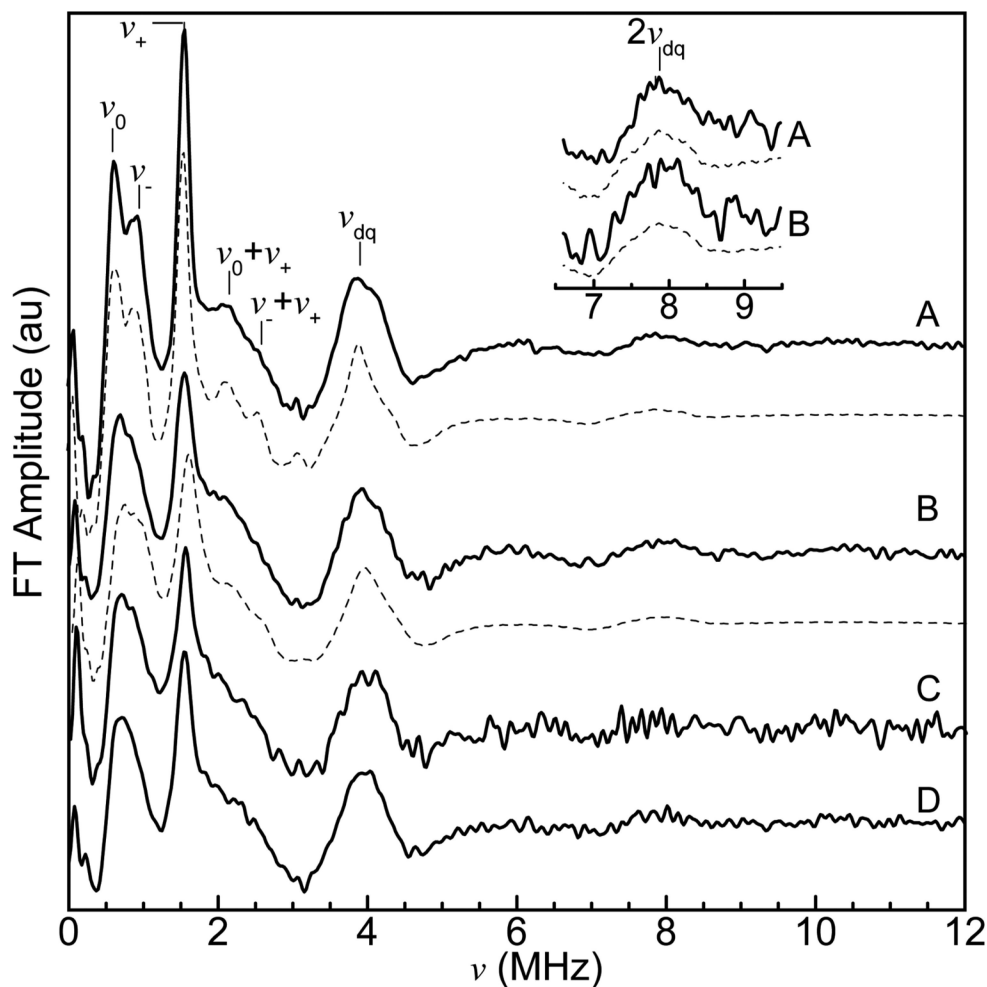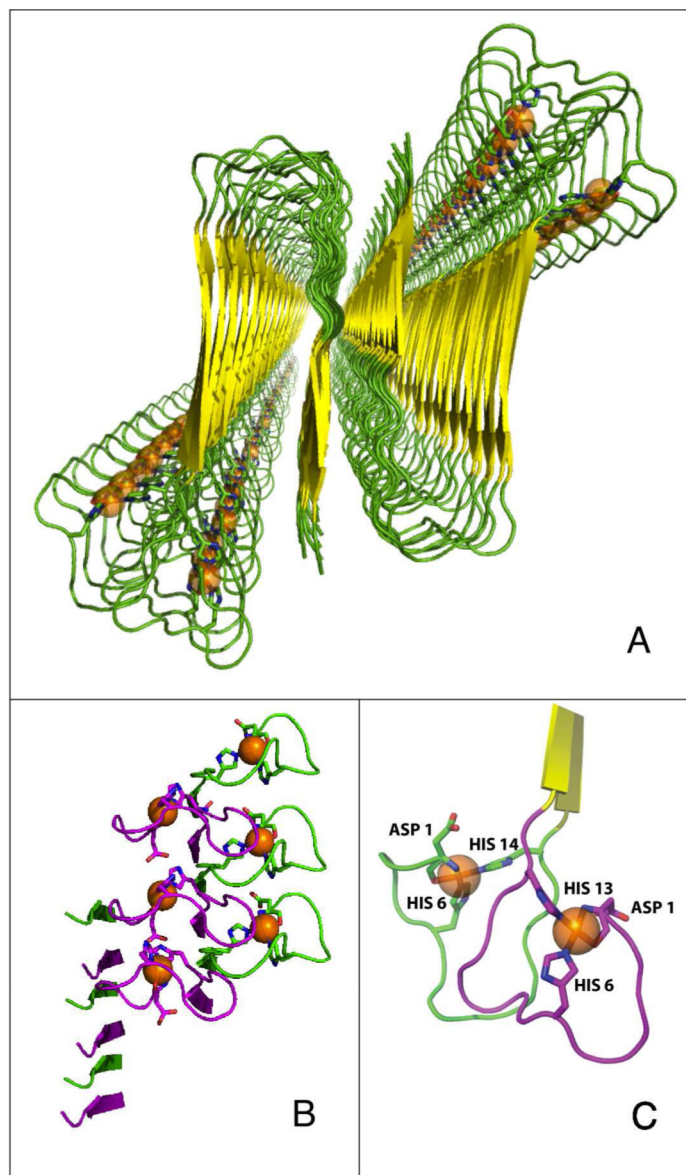
**Figure 3.**
FT spectra of the three-pulse ESEEM waveforms of $Cu^{2+}$-A$\beta$ complexes. (A) Soluble $Cu^{2+}$-A$\beta$(1-16), experiment and simulation (dashed line), (B) Fibrillar $Cu^{2+}$-A$\beta$(1-40), experiment and simulation (dashed line), (C) $^{13}C,^{15}N$-His13-$Cu^{2+}$-A$\beta$(1-40), (D) $^{13}C,^{15}N$-His14-$Cu^{2+}$-A$\beta$(1-40). Inset: Expanded view of double quantum harmonic region, for (A) soluble $Cu^{2+}$-A$\beta$(1-16) and (B) fibrillar $Cu^{2+}$-A$\beta$(1-40). *Acquisition Parameters*: microwave frequency, 8.750 GHz, $B_0 = 303$ mT, $T = 6$ K, $\tau = 310$ ns. Spectrum A is an average of 10 scans, spectrum B is an average of 16 scans, and spectra C and D are an average of 25 scans. Simulation parameters for spectra A and B are presented in Table 2.
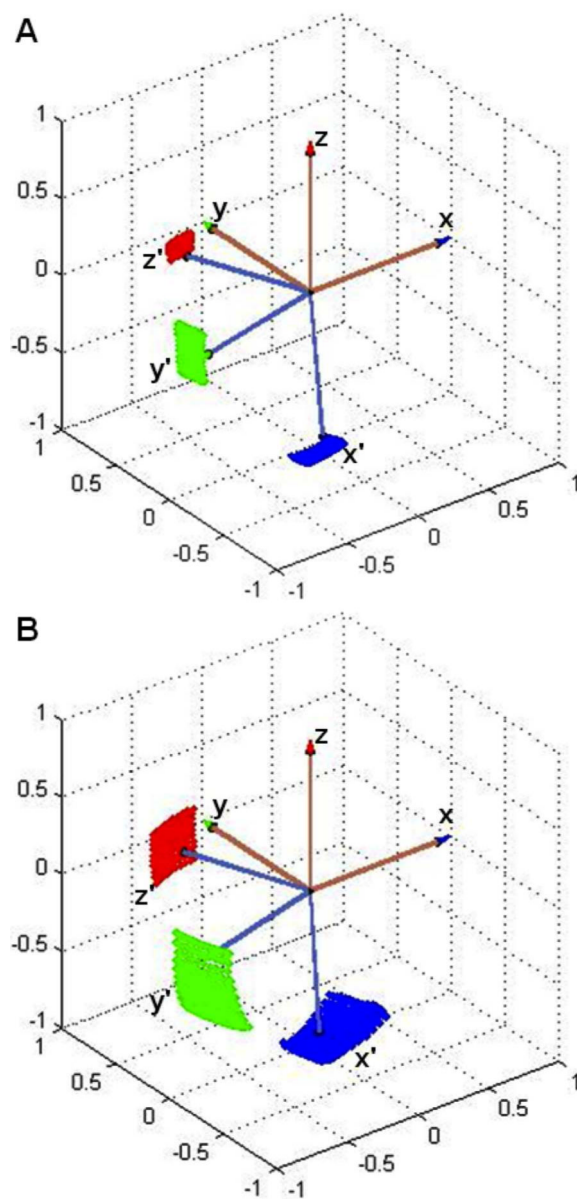
**Figure 4.**
Model for the mutual orientation of the histidine imidazole remote $^{14}N$ dipolar superhyperfine principal axis systems in (A) soluble $Cu^{2+}$-A$\beta$(1-16) and (B) fibrillar $Cu^{2+}$-A$\beta$(1-40). Figure axes represent the direction cosines, relative to the reference $x$, $y$, $z$-axis system (brown). The dotted surfaces show the 99% confidence interval, that corresponds to the Euler angles, $[\alpha_A, \beta_A, \gamma_A]$.

**Figure 5.**
Three-pulse ESEEM waveforms of (A) Fibrillar $Cu^{2+}$-Aβ(1-40), (B) $^{13}C,^{15}N$-His13-$Cu^{2+}$-Aβ(1-40), (C) $^{13}C,^{15}N$-His14-$Cu^{2+}$-Aβ(1-40), (D) envelope division; B divided by A, (E) envelope division; C divided by A. The vertical scale bar corresponds to 25% of the echo amplitude at $\tau + T = 8$ μs. *Aquisition Parameters*: microwave frequency, 8.750 GHz, $B_0 =$ 303 mT, $T = 6$ K, $\tau = 310$ ns.

**Figure 6.**
Model for the coordination of $Cu^{2+}$ in the fibrillar Aβ(1-40) peptide. The model is based on the quaternary structure for the ordered residues 9-40 of Aβ(1-40), which was determined by SS-NMR[3] (Protein Data Bank ID, 2LMN). (A) Protein secondary structure cartoon, showing global view down the fibril axis. The $Cu^{2+}$ ions are represented as orange spheres. (B) Side-on view of the N-terminal region, showing the patterning of $Cu^{2+}$ sites along the fibril axis. Purple and green loops represent His6/His13 and His6/His14 sites, respectively. (C) Local $Cu^{2+}$ coordination site geometry.
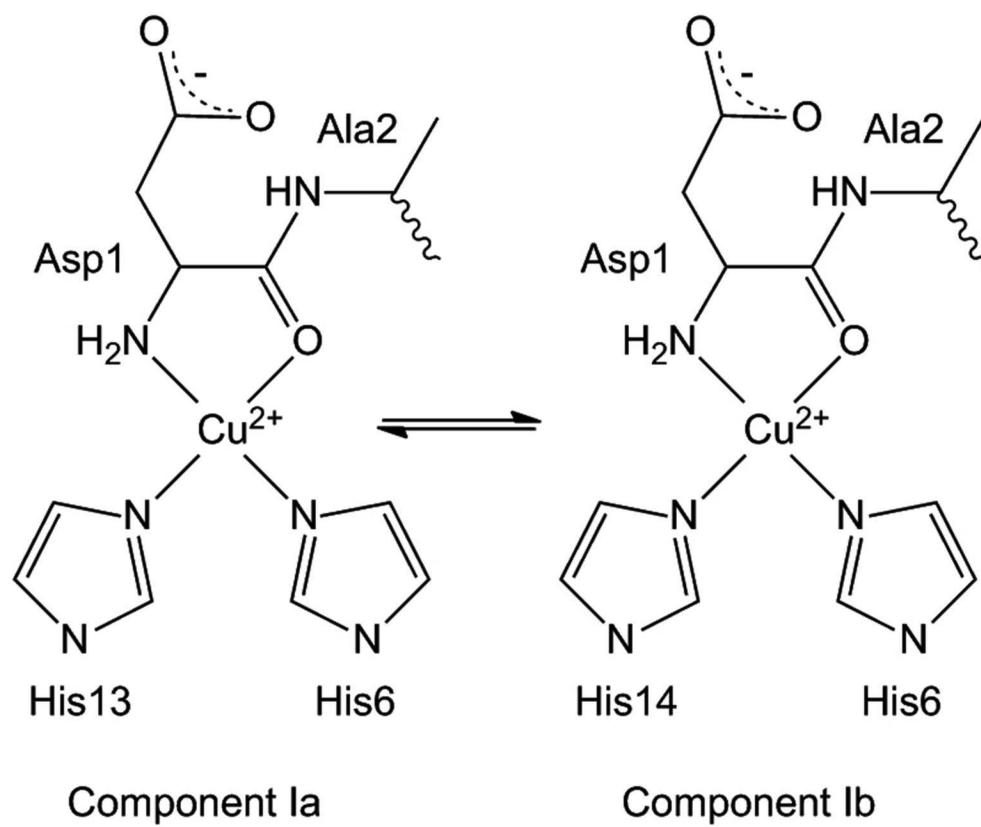
**Scheme 1.**

### Table 1

CW-EPR simulation parameters for the soluble, monomelic $Cu^{2+}$-A$\beta$(1-16) and fibrillar $Cu^{2+}$-A$\beta$(1-40) complexes.

| Parameter[a] | $Cu^{2+}$-A$\beta$(1-16) | $Cu^{2+}$-A$\beta$(1-40) |
|---|---|---|
| $g_\perp$ | 2.066 ±0.003 | 2.065 ±0.003 |
| $g_\parallel$ | 2.277 ±0.003 | 2.277 ±0.003 |
| $\sigma g_\perp$ | 0.030 | 0.031 |
| $\sigma g_\parallel$ | 0.025 | 0.026 |
| $A_\parallel$ (MHz)[b] | 524 ±5 | 527 ±5 |

[a]Simulations are for $S = 1/2$, $I = 3/2$, and have a Gaussian line width of 1.0 mT. Standard deviations are given.

[b]The copper hyperfine parameter ($A_\parallel$) is assumed to be from the $^{65}Cu$ isotope.

**Table 2**

ESEEM simulation parameters for the $Cu^{2+}$ coupling to the histidine imidazole remote $^{14}N$ nuclei in the soluble Aβ(1-16) and fibrillar Aβ(1-40) complexes.

| Parameters | $Cu^{2+}$-Aβ(1–16) | | $Cu^{2+}$-Aβ(1–40) | |
|---|---|---|---|---|
| | Values | 99% Confidence Interval | Values | 99% Confidence Interval |
| $A_{xx}$ (MHz) | 1.14 | 1.09-1.19 | 1.30 | 1.21-1.39 |
| $A_{yy}$ (MHz) | 1.74 | 1.70-1.76 | 1.76 | 1.70-1.80 |
| $A_{zz}$ (MHz) | 2.36 | 2.35-2.39 | 2.40 | 2.36-2.45 |
| $e^2Qq/h$ (MHz) | 1.59 | 1.57-1.59 | 1.57 | 1.56-1.59 |
| $\eta$ | 0.71 | 0.70-0.71 | 0.71 | 0.70-0.72 |
| $a_Q$ (°) | 357 | 354-359 | 0 | −5.40-16.6 |
| $\beta_Q$ (°) | 31.4 | 30.9-33.9 | 30.7 | 26.8-34.8 |
| $\gamma_Q$ (°) | 246 | 243-251 | 250 | 245-256 |
| $a_A$ (°) | 71.0 | 61.7-80.1 | 71.7 | 57.1-83.7 |
| $\beta_A$ (°) | 98.2 | 87.7-106 | 89.1 | 77.9-101.0 |
| $\gamma_A$ (°) | 1.70 | −6.1-6.2 | 0 | −24.0-13.8 |